Metastability of Constant-Density Flocks

Marc Besse,[1] Hugues Chaté,[2,3,1] and Alexandre Solon[1]
[1]Sorbonne Université, CNRS, Laboratoire de Physique Théorique de la Matière Condensée, 75005 Paris, France
[2]Service de Physique de l'Etat Condensé, CEA, CNRS Université Paris-Saclay, CEA-Saclay, 91191 Gif-sur-Yvette, France
[3]Computational Science Research Center, Beijing 100094, China

(Received 2 September 2022; accepted 6 December 2022; published 23 December 2022)

We study numerically the Toner-Tu field theory where the density field is maintained constant, a limit case of "Malthusian" flocks for which the asymptotic scaling of correlation functions in the ordered phase is known exactly. While we confirm these scaling laws, we also show that such constant-density flocks are metastable to the nucleation of a specific defect configuration, and are replaced by a globally disordered phase consisting of asters surrounded by shock lines that constantly evolves and remodels itself. We demonstrate that the main source of disorder lies along shock lines, rendering this active foam fundamentally different from the corresponding equilibrium system. We thus show that in the context of active matter also, a result obtained at all orders of perturbation theory can be superseded by nonperturbative effects, calling for a different approach.

DOI: 10.1103/PhysRevLett.129.268003

Understanding simple models and theories of collective motion emerging from spontaneous symmetry breaking has spurred the field of active matter, and largely continues to animate it. Emblematic in this context are the Vicsek model [1] and its field theoretical description, the Toner-Tu equations [2]. In spite of a lot of progress, several aspects of their asymptotic behavior are in fact still open problems. In particular, the original derivation of exact scaling relations for the correlation functions of the density and ordering (velocity) field in two dimensions (2D) [3] was later shown to rely on unduly neglecting some relevant terms [4]. Unsurprisingly, numerical measurements of correlation functions are inconsistent with the original prediction [5].

To make analytical progress, Toner and collaborators looked for simpler situations where the couplings between the conserved density field and the ordering field, which are at the origin of the difficulties mentioned above, are qualitatively modified. One such option is to tame the density field by considering "Malthusian flocks" in which particles die and reproduce on a fast scale [6–8]. Another is to introduce an incompressibility constraint [9,10]. In these two cases, remarkably, the scaling laws governing fluctuations of the ordered phase can be calculated at all orders of perturbation theory (in 2D for Malthusian flocks and any larger dimension for incompressible ones), providing rare examples of exact results about nontrivial out-of-equilibrium systems.

Incompressible and Malthusian flocks have otherwise received little attention. Rana and Perlekar have studied coarsening in the deterministic incompressible case [11,12]. The order-disorder transition in Malthusian flocks was approached using dynamical renormalization [13], and in a particle-based model [14].

Embarking on a numerical check of the exact results obtained by Toner *et al.* for the fluctuating ordered phase could appear as a waste of time. This is nevertheless what we did for Malthusian flocks, motivated mostly by recent results demonstrating the fragility of (usual, compressible) flocks to arbitrarily weak perturbations such as spatial anisotropy [15], quenched and chirality disorder [16–19], and even one small fixed obstacle [20]. More generally, results obtained at all orders in perturbation theory do not necessarily constitute the ultimate answer, since nonperturbative effects can always arise. Famous examples include the Kardar-Parisi-Zhang equation [21] and the Potts model in $6-\varepsilon$ dimensions [22,23].

Here we report on 2D numerical simulations of the Toner-Tu field theory in which the density field is maintained strictly constant, a limit case of Malthusian flocks. We find that while the predicted scaling laws are indeed obeyed by the homogeneous flocking phase, this phase is in fact always metastable to the nucleation of a specific defect configuration, leaving eventually a globally disordered cellular structure consisting of asters surrounded by shock lines that constantly evolves and remodels itself. The extended nature of these shock lines, across which the orientation of the field changes rapidly, renders this active foam fundamentally different from its equilibrium equivalent, the disordered phase of the XY model. We indeed show that the main source of disorder lies along and at the intersection of shock lines.

Our starting point is the following minimal active field theory with advection and alignment governing a single polarity or velocity field $\mathbf{v}$:

$$\partial_t \mathbf{v} + \lambda(\mathbf{v}\cdot\nabla)\mathbf{v} = \nabla^2\mathbf{v} + (a - |\mathbf{v}|^2)\mathbf{v} + \sqrt{2\eta}\boldsymbol{\xi}, \quad (1)$$

where $\boldsymbol{\xi}$ is a δ-correlated, unit-variance, zero-mean Gaussian white noise and two coefficients have been set to unity without loss of generality, leaving the three parameters a, λ, and the noise intensity η. One more parameter could be set to unity, but we retain these three to explore the different limits of the model. Equation (1) is the standard Toner-Tu theory where the density is kept constant, without imposing incompressibility. It can also be obtained from the field theory for Malthusian flocks by integrating out the fast density field, as done in Ref. [6]. Note that Eq. (1) is invariant under the transformation $\mathbf{v} \to -\mathbf{v}$ and $\lambda \to -\lambda$ [24]. In the following, we integrate Eq. (1) in 2D square domains of linear size L using a pseudo-spectral method with Euler explicit time stepping and antialiasing. We set the spatial resolution to $dx = 2$ and the time resolution to $dt = 0.1$, unless otherwise explicitly stated.

In 2D, Eq. (1) for $\lambda = 0$ reduces to the relaxational dynamics of a field theory describing the XY model. We thus expect a Berezinskii-Kosterlitz-Thouless (BKT) transition from disorder to quasi-long-range order (QLRO) when, say, increasing a [25,26]. On the other hand, the λ advection term controls the activity level and Toner predicts true long-range order (LRO) for large-enough a whenever $\lambda \neq 0$.

Simulating Eq. (1) with a large enough mass a from an ordered initial condition, the system indeed settles in a symmetry-broken state with nonzero mean velocity. We compute the order parameter $\bar{v} = \langle|\langle\mathbf{v}\rangle_{\mathbf{x}}|\rangle_t$ for various system sizes L ($\langle\cdot\rangle_{\mathbf{x}}$ and $\langle\cdot\rangle_t$ denote, respectively, space and time averages). In the passive limit $\lambda = 0$, we see $\bar{v}(L) \sim L^{-\theta}$, the signature of QLRO [a typical case is shown in Fig. 1 (left)]. The exponent θ varies continuously with a (not shown). Using its expected value $\theta = \frac{1}{8}$ at the BKT transition, we estimate the latter to happen at $a \simeq 0.38$. In the active case with not too small λ, in contrast, $\bar{v}(L)$ decays slower than a power law. As expected, our data are reasonably well fitted by $\bar{v} - \bar{v}_\infty \sim L^{-\omega}$, indicating LRO. Decreasing λ, this behavior is only observed beyond a crossover scale that seems to diverge when $\lambda \to 0$ [Fig. 1 (left)].

We further computed the scaling of velocity fluctuations via the structure factor, i.e., the Fourier transformed equal-time spatial correlation function $S_\perp(\mathbf{q}) = \langle|v_\perp(\mathbf{q},t)|^2\rangle_t$, where $v_\perp(\mathbf{q})$ is the velocity orthogonal to the direction of global order at wave vector $\mathbf{q} = (q_\perp, q_\parallel)$ [27]. Our results, shown in Fig. 1 (right), indicate anisotropic scaling in good quantitative agreement with the predictions of Toner in the small wave number limit: $S_\perp(q_\parallel) \sim |q_\parallel|^{-2}$ if $q_\parallel \gg q_\perp$ and $S_\perp(q_\perp) \sim |q_\perp|^{-6/5}$ if $q_\perp \gg q_\parallel$ [6].

The agreement between our measurements and the theoretical prediction is hardly surprising. However, as

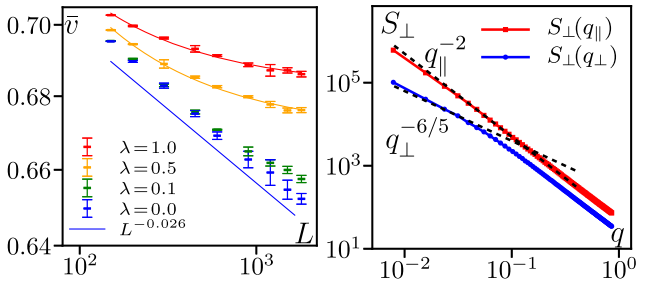

FIG. 1. Left: $\bar{v}(L)$ for different λ values ($a = 0.7$, $\eta = 0.5$ and initial ordered state). Error bars correspond to two standard errors of the mean computed over five independent samples. For large λ values, $\bar{v}(L)$ is reasonably well fitted by $\bar{v} - \bar{v}_\infty = AL^{-\omega}$ with $\omega = 2/3$ ($\bar{v}_\infty = 0.67$, $A = 0.77$, for $\lambda = 0.5$, orange curve, and $\bar{v}_\infty = 0.68$, $A = 0.57$, for $\lambda = 1.0$, red curve). Right: $S_\perp$ versus $q_\parallel$ for $q_\perp = 0$ (red squares) and versus $q_\perp$ for $q_\parallel = 0$ (blue dots) ($a = 5$, $\lambda = 1$, $\eta = 0.5$, $L = 800$). Dashed lines: scaling predicted at small wave vectors [6], which arises only beyond a crossover scale for $S_\perp(q_\perp)$. Averages are taken over a time 10^6 small enough that the nucleation events described in Fig. 2 are not observed.

we show now, this is far from being the whole story. For not too large a values, in a large-enough system, the ordered phase described above is easily observed to break down spontaneously: fluctuations can lead to the emergence of a specific local configuration made of an aster surrounded by a semicircular shock line [Fig. 2(a)]. The aster is a point around which polarity is arranged radially, where a $+1$ topological defect is thus located. Across the shock line, polarity varies rapidly. It actually embeds a -1 defect as we will see later. In large systems, this initial nucleation is followed by others located elsewhere and/or the emergence of new asters (and their accompanying shock lines) along the shock line of the initial aster [Fig. 2(b)]. Eventually, proliferation stops and a globally disordered, dynamical state is reached, with a well-defined average number of asters and a web of shock lines surrounding them [Figs. 2(c) and 2(d) and Movie 1 in Ref. [28]]. In this steady state, new asters are constantly generated near shock lines—dominantly near their intersections—while existing asters see their position and size fluctuate until one of their surrounding shock lines meets their center, at which point they disappear.

We studied the statistics of the nucleation process of the first aster from the ordered phase. Figure 2(e) shows that the lifetime τ of the ordered phase, i.e., the time it takes for nucleation events to happen, is distributed exponentially with a characteristic time that scales roughly like $1/L^2$, the inverse system size. In other words, the nucleation rate is proportional to L^2. This confirms that the emergence of asters and their surrounding shock line is essentially a local nucleation process, even though the ordered phase possesses built-in long-range correlations. Replicating this Letter at higher values of a quickly becomes numerically prohibitive because τ can then take very large values.

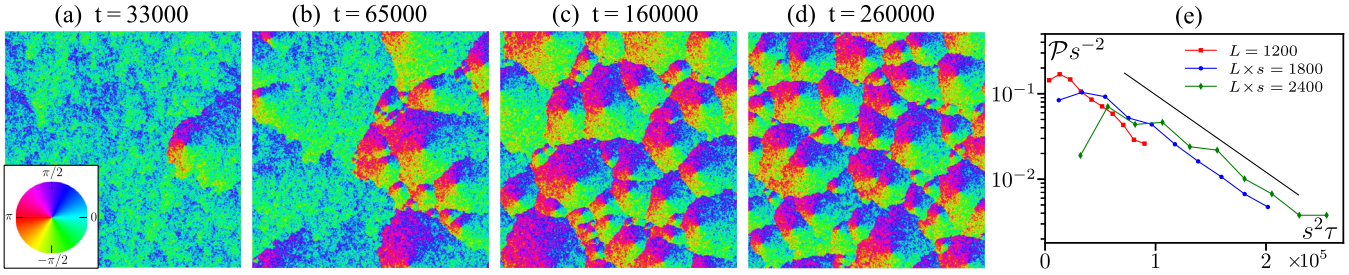

FIG. 2. (a)–(d) Snapshots taken during a run starting from an ordered state showing the nucleation of a first defect and the following evolution ($a = 0.48$, $\lambda = 1.0$, $\eta = 0.5$, $L = 3600$). (e) Probability distribution $\mathcal{P}$ of the lifetime of the ordered phase τ, defined as the first time for which the nucleation of an aster decreases $\bar{v}$ by more than 20% ($a = 0.45$, $\lambda = 1.0$, $\eta = 0.5$). Data obtained at three different L values, rescaled by a factor s^2 proportional to L^2.

We now study directly the dynamic active foam. This steady state is easily reached from disordered initial conditions after a typically short coarsening transient (cf. Movie 2 in Ref. [28]). This allows us to study it at parameter values for which the spontaneous nucleation of an aster from the ordered phase would take unreasonably long times. The active foam can be characterized by its average number of asters, but we preferred to measure the more robust correlation length ξ extracted from the azimuthally averaged structure factor [29]. At fixed parameters, ξ converges to a well-defined asymptotic value when the system size L is increased: the active foam is self-averaging, and reliable estimates of its intrinsic correlation length are obtained as soon as $L \gg \xi$. At fixed activity λ, we find that ξ increases with increasing a, but this growth is modest, possibly linear with a (Fig. 3, left). Contrary to the passive case where the BKT transition at $a \simeq 0.38$ marks the fast divergence of correlations, we do not see any sign of a transition beyond which the ordered phase would remain stable. Extrapolating our numerical results, we conclude that the ordered phase is metastable for any nonzero λ [30] and positive a (ignoring a possible renormalized value for the $a = 0$ mean-field threshold), even if at large a values it can be stable for a long enough time to measure its properties, such as in Fig. 1.

To better understand why the active regime is so different from the passive case, we now turn to a more detailed study of the objects at play in the dominating active foam phase, i.e., asters and shock lines.

Asters have been reported in models of the self-organization of microtubules and molecular motors [31–34], but also in variants of the Toner-Tu equations [32,35–38], as well as in active gel theory [39,40]. All these systems are more complex than ours, including a density and/or a motor concentration field. To the best of our knowledge, only Vafa [41] studied defects in the simple equation (1) of interest here, concluding that asters are the most stable $+1$ defects [42]. This result is in agreement with our observations of the active foam, where asters are quite passive regions, and most of the remaining activity occurs at the shock lines and, in particular, at their intersection (cf. Movies 1 and 2 in Ref. [28]).

Active foam configurations are best understood in the deterministic version of Eq. (1), either by switching off the noise from a given configuration or by watching the slow coarsening following disordered initial conditions (cf. Movie 3 in Ref. [28]) [43]. The right-hand panel of Fig. 3 shows a late configuration comprising a few remaining asters and their surrounding shock lines, extracted from this coarsening process. Close inspection shows that shock lines are extended objects across which

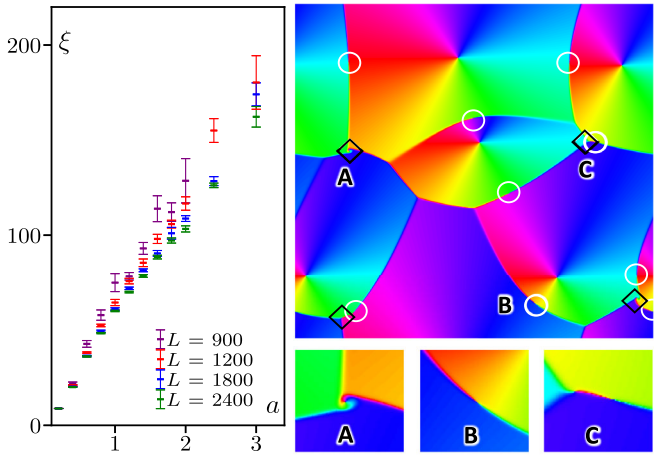

FIG. 3. Left: variation of correlation length ξ with a for different sizes L. Data taken in the active foam steady state ($\lambda = 1.0$, $\eta = 0.5$). Error bars correspond to 2 standard errors of the mean, computed over 10 independent time intervals, each much longer than the correlation time of the global velocity. At a given a value, small size data may not be reliable since ξ can then be of the order of L. At $L = 900$ in particular, data for $a > 2.0$ are not shown since only very few or even no asters are present. Right: typical configuration taken during coarsening in the deterministic limit $\eta = 0$ [$a = 1$, $\lambda = 1.0$, $L = 900$, $dx = 0.5$, $dt = 0.01$, colors as in Fig. 2(a), from Movie 3 in Ref. [28]]. Apart from the five clearly visible asters, which have $+1$ topological charge, nine shock-line embedded -1 defects are present (white circles), as well as four vortexlike $+1$ defects present at some shock line vertices (black diamonds). Labels A, B, and C in the main panel point to the defects shown more clearly in the small lower panels.

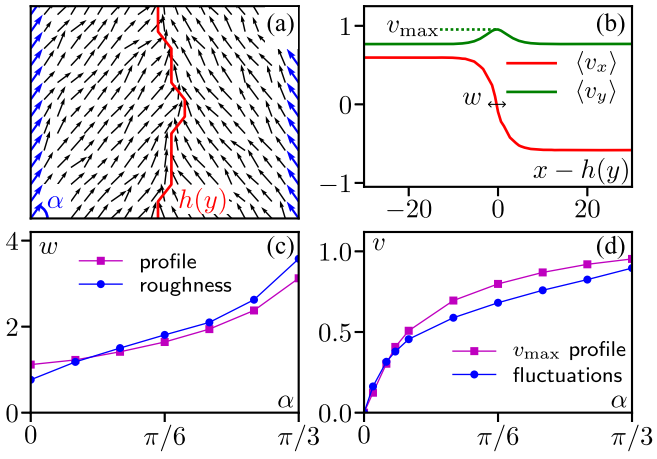

FIG. 4. Study of the interface $h(y)$ separating two half domains with different bulk orientation ($a = 1$, $\lambda = 1$, $\eta = 0.1$, periodic boundary condition in y). (a) Typical snapshot showing $h(y)$ (red line) defined by the points along x where v_x changes sign (300×100 system). Velocity is fixed symmetrically on lateral boundaries at an angle $\alpha = \pi/3$ (blue arrows). (b) Mean horizontal profiles of v_x and v_y measured relative to the interface position $h(y)$, averaged over y and time. (c) Variation with α of the width of the interfacial region, measured either by fitting the average profile $\langle v_x \rangle$ [as in (b)] by a tanh function (magenta squares) or as the roughness of the interface $w = \sqrt{\langle \langle h^2 \rangle_y - \langle h \rangle_y^2 \rangle_t}$ (blue circles). System size 100×100. (d) Same as (c) but showing the propagation speed of fluctuations along the interface obtained either as the maximum of $\langle v_y \rangle$ in (b) (magenta squares) or from the space-time Fourier transformed correlation function $\langle |h(q_y, \omega)^2| \rangle_t$ as the position of the peaks $\omega = v q_y$ at small wave vector q_y.

the phase varies rapidly but not discontinuously. Given the existence of $+1$ defects (at the centers of asters), -1 defects must be present. In the five-aster configuration under scrutiny, nine defects with topological charge -1 are found embedded in the shock lines (white circles, enlargement B), typically located at the locations closest to the aster centers, where the phase jump is $\pm\pi$. The -2π circulation around these defects is mostly due to two phase jumps occurring when crossing the shock line. This suggests that the important structures are the shock lines and not the pointwise -1 defects. Given that the global topological charge must be zero, our inspection is not complete. Indeed one can locate four other $+1$ vortexlike defects located at shock lines vertices (black diamonds, enlargements A and C). Note finally that the shock line vertices are rather unstable dynamically, even in the absence of noise (cf. Movie 3 [28]), although in that case the coarsening proceeds all the way to the ordered state.

Coming back to the noisy case, the radially organized aster regions appear rather stable—in agreement with Vafa's findings [41]—and the strongest fluctuations are found along shock lines (Movies 1 and 2 in Ref. [28]). We studied these fluctuations in specially prepared systems with a single shock line separating two large ordered homogeneous domains whose orientations differ by some angle $\pi - 2\alpha$ [Fig. 4(a)]. The profile of the interface, shown in Fig. 4(b), is close to its deterministic shape. Under the effect of noise the interface fluctuates. Its roughness increases monotonically with α, and so does the width of the mean profile [Fig. 4(c)]. For $\alpha > 0$, parity symmetry is broken along the interface, and fluctuations on the shock line are advected along the direction given by the sign of $\langle v_y \rangle$. We find that the advection speed of fluctuations increases with α in the same way as the maximum of $\langle v_y \rangle$ [Fig. 4(d)].

In typical configurations such as those shown in Figs. 2(a)–2(d) and 3(b), the local orientation difference across a shock line varies with the position along the line. In the notation introduced above, near the intersection with the line joining the two aster centers (where a -1 defect typically sits), the phase jump corresponds to $\alpha \simeq 0$ while going away from this point means increasing α. Using the results obtained in Fig. 4 with constant-α shock lines, we can now understand why fluctuations are growing and are advected faster and faster when going away from the $\alpha \simeq 0$ point. They are maximal at shock line intersections, making these regions the most unstable ones where new asters are created. Thus the mechanisms maintaining the active foam in a steady state are intimately linked to the extended nature of shock lines.

In conclusion, we have shown numerically that fluctuations in the ordered phase of the 2D constant-density Toner-Tu theory obey the scaling laws predicted by a renormalization group analysis, but we have also found that these flocks are metastable to an ever-evolving active foam made of asters surrounded by a network of shock lines in a large region of parameter space. While we cannot rule out in principle a divergence of the correlation length or a sudden vanishing of defect proliferation mechanisms at parameter values unexplored here, we find no indication of either scenario. On the contrary, our demonstration that shock lines separating asters are crucial to amplify and advect perturbations, and that the vertices of the network they form are the most susceptible regions of space where new asters are created, should remain valid at all parameter values.

Our findings constitute an instance, in the context of active matter, where a result obtained at all orders of perturbation theory is superseded by nonperturbative effects, calling for a different approach.

The topology and dynamics of the structures at play are qualitatively different from the binding or unbinding of pairs of point defects that rules the fate of order in the passive case of the XY model. This is reminiscent of the recent study of coarsening in the compressible case, where a network of "domain walls" was put forward but no asters are present [44]. Coarsening was also studied in the incompressible case, but there the dominating structures are standard vortices and antivortices [11]. The objects at

play in defected flocking systems can thus vary qualitatively, an observation that calls for further study.

The field theory studied here is a limit case of that for Malthusian flocks, where a fast but finite timescale regulates the density field. It would be interesting to see how our results translate to this more general setting, including in microscopic, particle-level models. Future work should also investigate the possibility of similar "nonperturbative metastability" of long-range orientational order in other important models and field theories of active matter both in 2D and 3D.

Finally, our findings could be of relevance in some real systems in spite of the simplicity of the framework we considered. Prime candidates are found in cytoskeletal active matter, i.e., *in vitro* mixtures of (mostly) biofilaments and molecular motors, for which the formation of asters has been reported [45–53].

We thank Matthieu Tissier for insightful discussions and Francesco Ginelli, Benoît Mahault, and Xia-qing Shi for their comments on the manuscript. The work of H. C. was supported in part by ANR project NeqFluids Grant No. ANR-18-CE92-0019 and the National Natural Science Foundation of China (Grant No. 11635002).

[1] T. Vicsek, A. Czirók, E. Ben-Jacob, I. Cohen, and O. Shochet, Phys. Rev. Lett. **75**, 1226 (1995).
[2] J. Toner and Y. Tu, Phys. Rev. Lett. **75**, 4326 (1995).
[3] J. Toner and Y. Tu, Phys. Rev. E **58**, 4828 (1998).
[4] J. Toner, Phys. Rev. E **86**, 031918 (2012).
[5] B. Mahault, F. Ginelli, and H. Chaté, Phys. Rev. Lett. **123**, 218001 (2019).
[6] J. Toner, Phys. Rev. Lett. **108**, 088102 (2012).
[7] L. Chen, C. F. Lee, and J. Toner, Phys. Rev. Lett. **125**, 098003 (2020).
[8] L. Chen, C. F. Lee, and J. Toner, Phys. Rev. E **102**, 022610 (2020).
[9] L. Chen, J. Toner, and C. F. Lee, New J. Phys. **17**, 042002 (2015).
[10] L. Chen, C. F. Lee, and J. Toner, New J. Phys. **20**, 113035 (2018).
[11] N. Rana and P. Perlekar, Phys. Rev. E **102**, 032617 (2020).
[12] N. Rana and P. Perlekar, Phys. Rev. E **105**, L032603 (2022).
[13] L. Di Carlo and M. Scandolo, arXiv:2202.01010.
[14] P. K. Mishra and S. Mishra, Phys. Fluids **34**, 057110 (2022).
[15] A. Solon, H. Chaté, J. Toner, and J. Tailleur, Phys. Rev. Lett. **128**, 208004 (2022).
[16] J. Toner, N. Guttenberg, and Y. Tu, Phys. Rev. Lett. **121**, 248002 (2018).
[17] J. Toner, N. Guttenberg, and Y. Tu, Phys. Rev. E **98**, 062604 (2018).
[18] Y. Duan, B. Mahault, Y.-q. Ma, X.-q. Shi, and H. Chaté, Phys. Rev. Lett. **126**, 178001 (2021).
[19] B. Ventejou, H. Chaté, R. Montagne, and X.-q. Shi, Phys. Rev. Lett. **127**, 238001 (2021).
[20] J. Codina, B. Mahault, H. Chaté, J. Dobnikar, I. Pagonabarraga, and X.-q. Shi, Phys. Rev. Lett. **128**, 218001 (2022).
[21] K. J. Wiese, J. Stat. Phys. **93**, 143 (1998).
[22] D. J. Amit, J. Phys. A **9**, 1441 (1976).
[23] R. Priest and T. Lubensky, Phys. Rev. B **13**, 4159 (1976).
[24] For simplicity, we do not include the two advection terms $(\nabla \cdot \mathbf{v})\mathbf{v}$ and $\nabla(|\mathbf{v}|^2)$ and the bulk viscosity term $\nabla(\nabla \cdot \mathbf{v})$. We checked that their presence does not modify our results.
[25] V. Berezinskii, Sov. Phys. JETP **32**, 493 (1971).
[26] J. M. Kosterlitz and D. J. Thouless, J. Phys. C **6**, 1181 (1973).
[27] Time averaging is delicate because the direction of global order drifts slowly. Following Ref. [5], we apply an external field large enough to pin the global direction of order but small enough that it does not affect the correlation functions on the range of q values displayed.
[28] See Supplemental Material at http://link.aps.org/supplemental/10.1103/PhysRevLett.129.268003 for supplementary movies.
[29] $\xi = 2\pi \int dq S(q) / \int dq q S(q)$ with $q = |\mathbf{q}|$.
[30] Partial results indicate that both τ and ξ diverge as $\lambda \to 0$.
[31] H. Y. Lee and M. Kardar, Phys. Rev. E **64**, 056113 (2001).
[32] S. Sankararaman, G. I. Menon, and P. B. Sunil Kumar, Phys. Rev. E **70**, 031905 (2004).
[33] I. S. Aranson and L. S. Tsimring, Phys. Rev. E **71**, 050901(R) (2005).
[34] I. S. Aranson and L. S. Tsimring, Phys. Rev. E **74**, 031915 (2006).
[35] A. Gopinath, M. F. Hagan, M. C. Marchetti, and A. Baskaran, Phys. Rev. E **85**, 061903 (2012).
[36] K. Gowrishankar and M. Rao, Soft Matter **12**, 2040 (2016).
[37] K. Husain and M. Rao, Phys. Rev. Lett. **118**, 078104 (2017).
[38] J. Elgeti, M. E. Cates, and D. Marenduzzo, Soft Matter **7**, 3177 (2011).
[39] K. Kruse, J. F. Joanny, F. Jülicher, J. Prost, and K. Sekimoto, Phys. Rev. Lett. **92**, 078101 (2004).
[40] K. Kruse, J. F. Joanny, F. Jülicher, J. Prost, and K. Sekimoto, Eur. Phys. J. E **16**, 5 (2005).
[41] F. Vafa, arXiv:2009.10723.
[42] Note that asters are pointing outward with $\lambda > 0$, and inward when with $\lambda < 0$.
[43] In the deterministic case, we believe, in agreement with Vafa [41], that coarsening proceeds all the way to the ordered phase; in practice, finite resolution may pin the system in some near-final configuration with few asters.
[44] A. Chardac, L. A. Hoffmann, Y. Poupart, L. Giomi, and D. Bartolo, Phys. Rev. X **11**, 031069 (2021).
[45] F. Nédélec, T. Surrey, A. C. Maggs, and S. Leibler, Nature (London) **389**, 305 (1997).
[46] T. Surrey, F. Nédélec, S. Leibler, and E. Karsenti, Science **292**, 1167 (2001).
[47] F. Backouche, L. Haviv, D. Groswasser, and A. Bernheim-Groswasser, Phys. Biol. **3**, 264 (2006).
[48] C. Hentrich and T. Surrey, J. Cell Biol. **189**, 465 (2010).
[49] P. A. Nguyen, A. C. Groen, M. Loose, K. Ishihara, M. Wühr, C. M. Field, and T. J. Mitchison, Science **346**, 244 (2014).

[50] S. Stam, S. L. Freedman, S. Banerjee, K. L. Weirich, A. R. Dinner, and M. L. Gardel, Proc. Natl. Acad. Sci. U.S.A. **114**, E10037 (2017).

[51] N. Khetan, G. Pruliere, C. Hebras, J. Chenevert, and C. A. Athale, J. Cell Sci. **134**, jcs257543 (2021).

[52] J. Berezney, B. L. Goode, S. Fraden, and Z. Dogic, Proc. Natl. Acad. Sci. U.S.A. **119**, e2115895119 (2022).

[53] B. Lemma, N. P. Mitchell, R. Subramanian, D. J. Needleman, and Z. Dogic, Phys. Rev. X **12**, 031006 (2022).